Palaeogeography, Palaeoclimatology, Palaeoecology 505 (2018) 359–370

Contents lists available at ScienceDirect

Palaeogeography, Palaeoclimatology, Palaeoecology

journal homepage: www.elsevier.com/locate/palaeo

# Relationship between magnetic susceptibility and sediment grain size since the last glacial period in the Southern Ocean off the northern Antarctic Peninsula – Linkages between the cryosphere and atmospheric circulation

Sunghan Kim*, Kyu-Cheul Yoo, Jae Il Lee, Min Kyung Lee, Kitae Kim, Ho Il Yoon, Heung Soo Moon

*Korea Polar Research Institute, Incheon 21990, Republic of Korea*

ARTICLE INFO

*Keywords:*
Magnetic susceptibility
Grain size
Ice-rafted debris
Southern ocean
The last glacial period

ABSTRACT

Magnetic susceptibility (MS) values in Scotia Sea sediments showed strong correlations to ice core non-sea salt $Ca^{2+}$ concentration (dust input), which emphasizes the role of atmospheric circulation in the Southern Ocean. As a result, the correlation between these values was suggested as a powerful tool for age reconstruction of marine sediments in the Southern Ocean. However, controls on MS variation in Scotia Sea sediments are not clear. In this study, we documented records of grain size, MS values ($10^{-6}$ CGS/g) of bulk sediments, and MS values of sand-sized (> 63 μm), coarse silt-sized (16–63 μm), and fine sediment fractions (< 16 μm) at sediment cores from the Southern Ocean off the northern Antarctic Peninsula (the south Scotia Sea and the northern Powell Basin) to reveal which size fraction is responsible for increased MS values during the glacial period and how this size fraction is transported to the Southern Ocean deep-sea. The MS values of all cores GC02-SS02, GC03-C2, GC03-C4, and GC04-G03 increased along with increased sand- and coarse silt-sized fractions and decreased fine sediment fraction. Although The MS values of all size fractions increased during the glacial period, the increased glacial MS values are more related to fine sand- to coarse silt-sized fractions than they are to the fine sediment fraction. The fine sand- to coarse silt-sized sediments with the highest MS values during the glacial period show (semi-)normal distribution patterns, indicating that they are transported by the same mechanism. The sediments are considered to be transported as ice rafted debris (IRD) during the glacial period. Based on our record, the strong correlation between marine core MS values and ice core dust record thus suggests a strong linkage between the cryosphere (iceberg calving activity) and atmospheric circulation (dust) in the Southern Ocean off the northern Antarctic Peninsula.

## 1. Introduction

The Southern Ocean plays an important role in global climate changes through deep-water formation (Orsi et al., 1995) and the biological pump (Takahashi et al., 2002). However, paleoclimatic/paleoceanographic studies in the Southern Ocean have a chronic problem with age reconstruction due to lack of foraminifers and the influence of old carbon (Gordon and Harkness, 1992; Nakada et al., 2000; Anderson et al., 2002; Heroy and Anderson, 2005; The RAISED Consortium et al., 2014). It was reported that magnetic susceptibility (MS) records in Scotia Sea sediments were well correlated with the non-sea salt $Ca^{2+}$ ($nssCa^{2+}$) concentration, a proxy for dust input (Röthlisberger et al., 2004; Lambert et al., 2011), of the European Project for Ice Coring in Antarctica (EPICA) Drauning Maud Land (EDML) ice core (Weber et al., 2012; Xiao et al., 2016 and references therein). Through graphical correlation between MS records of sediment cores in the Scotia Sea and EDML ice core $nssCa^{2+}$ record, high-resolution age reconstructions for sediment cores became possible and the established age models were consistent with other stratigraphic data (Pugh et al., 2009; Allen et al., 2011; Weber et al., 2012; Xiao et al., 2016).

Considering the importance of MS for sediment age establishment, it is essential to understand the controlling mechanism of MS in marine sediments in the Scotia Sea. Although Patagonia/southern South America is the main dust source region for the Antarctic continent (Haberzettl et al., 2009), the mechanisms transporting fine sediments to the Scotia Sea remain controversial (Hofmann, 1999; Diekmann et al., 2000; Pugh et al., 2009; Weber et al., 2012). Since the magnetic properties of marine sediments are often associated with grain size changes (Evans and Heller, 2003), grain size changes should be examined for MS variations in the Scotia Sea. Grain size changes in the

* Corresponding author.
*E-mail address:* delongksh@kopri.re.kr (S. Kim).

https://doi.org/10.1016/j.palaeo.2018.06.016
Received 27 December 2017; Received in revised form 30 May 2018; Accepted 8 June 2018
Available online 15 June 2018

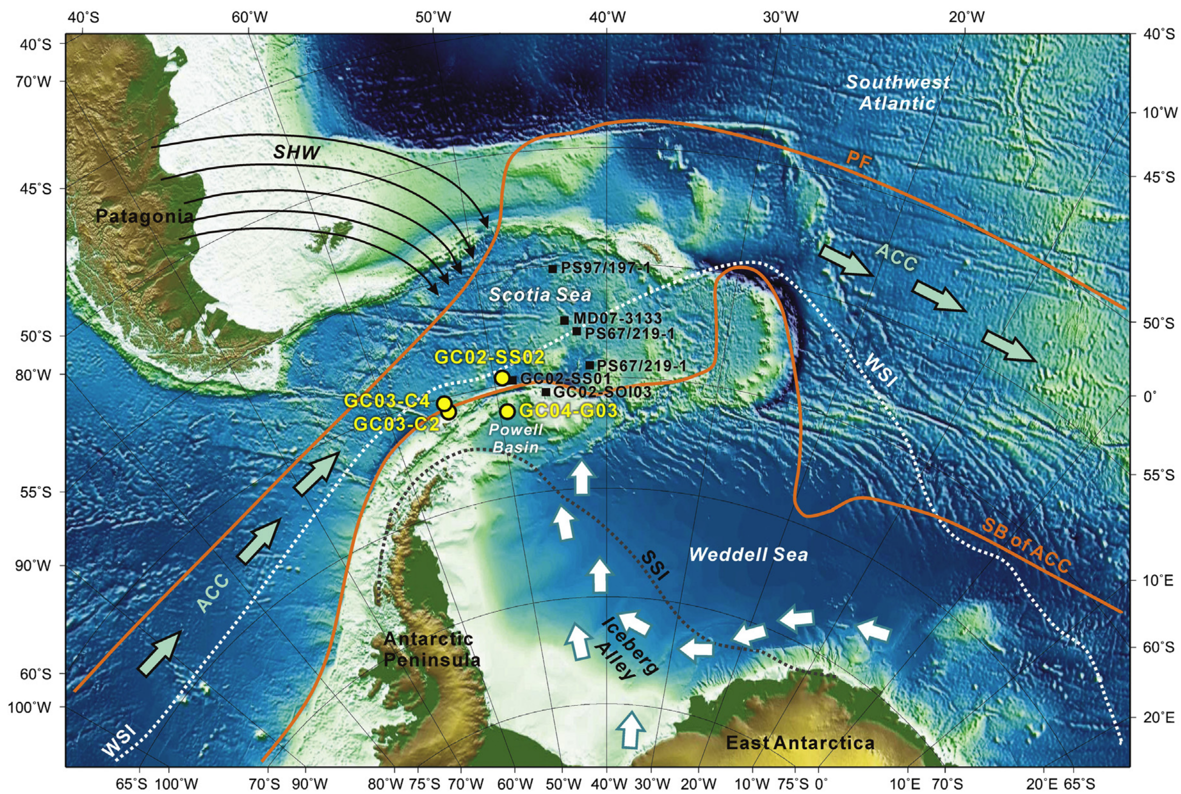


**Fig. 1.** Site location map with cores examined in this study and previous studies. White open arrows indicate iceberg alley of Anderson and Andrew (1999). Black arrows indicate the main wind direction of Southern Hemisphere Westerlies (SHW). Polar Front (PF) and Southern Boundary of Antarctic Circumpolar Current (SB of ACC; Orsi et al., 1995) are indicated by orange lines. The dark gray and white dashed lines are the summer (SSI) and winter (WSI) sea ice extent, respectively (Gersonde et al., 2005). ACC is shown by light green arrows. Information on core locations is listed in Table 1.

**Table 1**
Information on cores shown in Fig. 1.

| Core ID | Latitude | Longitude | Water depth (m) | Source |
|---|---|---|---|---|
| GC02-SS02 | 59°29′S | 49°36′W | 4033 | This study |
| GC03-C2 | 60°34′S | 55°55′W | 3750 | This study |
| GC03-C4 | 60°33′S | 55°52′W | 3778 | This study |
| GC04-G03 | 61°19′S | 49°48′W | 2907 | This study |
| GC02-SS01 | 59°49′S | 49°14′W | 4141 | Yoon et al., 2005 |
| GC02-SOI03 | 60°22′S | 47°00′W | 786 | Lee et al., 2010 |
| MD07-3133 | 57°26′S | 43°27′W | 3101 | Weber et al., 2012 |
| MD07-3134 | 59°25′S | 41°28′W | 3663 | Weber et al., 2012 |
| PS2319-1 | 59°47′S | 42°41′W | 4320 | Diekmann et al., 2000 |
| PS2515-3 | 53°33′S | 45°19′W | 3522 | Diekmann et al., 2000 |
| PS67/197-1 | 55°08′S | 44°06′W | 3837 | Xiao et al., 2016 |
| PS67/219-1 | 57°57′S | 42°28′W | 3619 | Xiao et al., 2016 |

Scotia Sea have been rarely reported (e.g., Yoon et al., 2005), and the relationship between changes of MS and grain size has not been discussed previously.

The modern Southern Ocean off the northern Antarctic Peninsula, including the south Scotia Sea and the Powell Basin, is located in the core of iceberg alley (Fig. 1), which originates in the Weddell Sea (Reid and Anderson, 1990; Diekmann and Kuhn, 1999). As sea ice and an ice sheet expanded during the last glacial period (Gersonde et al., 2005; Larter et al., 2014; Minzoni et al., 2015), more ice-rafted debris (IRD) was found in the marine sediments in the Southern Ocean (Diekmann et al., 2000; Hillenbrand et al., 2005). However, IRD (> 2 mm) abundance was not correlated to high MS values of Scotia Sea sediment cores during the last glacial period. IRD is not only limited to gravel-sized particles but also sand-sized grains are transported by icebergs (Andrews, 2000; Jonkers et al., 2012, 2015). Indeed, sand size grains (63–150 μm to 2 mm) were considered IRD in high-latitude deep-sea areas in both the Southern and Northern Hemispheres (e.g., Kanfoush et al., 2000; Sakamoto et al., 2005, 2006; Peck et al., 2007, 2015; Bailey et al., 2013; Teitler et al., 2015). Thus, it is necessary to re-examine the role of IRD in MS variation in the Southern Ocean off the northern Antarctic Peninsula using new representative IRD size criteria.

In this study, we document grain size distributions and MS values of the Southern Ocean off the northern Antarctic Peninsula to 1) determine which size fraction is related to MS variation since the last glacial period and 2) define the transport mechanism for this size fraction. An additional purpose is to provide the most suitable size criteria for IRD in the Southern Ocean deep-sea cores.

## 2. Materials and methods

A gravity core GC02-SS02 (59°29′S, 49°36′W, 4033 m deep, 478 cm long) was obtained from the south Scotia Sea by R/V *Yuzhmorgeologiya* during the 2002/2003 Korea Antarctic Research Program (KARP) cruise (Fig. 1, Table 1). Gravity cores GC03-C2 (60°34′S, 55°55′W, 3750 m deep, 834 cm long), GC03-C4 (60°33′S, 55°52′W, 3778 m deep, 840 cm long), and a box core BC03-C2 (60°34′S, 55°55′W, 3750 m deep, 38 cm long) were obtained from the south Scotia Sea by R/V *Yuzhmorgeologiya* during 2003/2004 KARP Cruise (Fig. 1, Table 1). A gravity core GC04-G03 (61°19′S, 49°48′W, 2907 m deep, 596 cm long) was obtained from the northern part of the Powell Basin by R/V *Yuzhmorgeologiya* during 2004/2005 KARP Cruise (Fig. 1, Table 1). All cores were opened, described, and sub-sampled at the Korea Polar Research Institute (KOPRI).

### *2.1. Physical properties (magnetic susceptibility and water content measurement)*

The MS values for all sediment cores were measured at 1 cm intervals on split half core sections using a Bartington MS-2B susceptibility meter at KOPRI. The MS values of core GC02-SS02 were previously reported in Yoon et al. (2005). The MS values were also measured from bulk samples, and > 63 μm (sand-sized), 16–63 μm (5–6 phi; coarse silt-sized), and < 16 μm (7–11 phi; fine sediment) size fractions of dried sediments from a high MS interval (750–840 cm) and a low MS interval (140–180 cm) at core GC03-C4 using a Bartington MS-2B susceptibility meter at KOPRI. In addition, the MS values of 250–63 μm grains were measured at core GC04-G03 using a Bartington MS-2B susceptibility meter at KOPRI.

Water content (WC) was measured for the top 100 cm of cores GC03-C2 and core BC03-C2 to correct the core top loss of GC03-C2 by the following equation:

$$\mathrm{WC}\ (\%) = (\text{mass of wet sediment} - (\text{mass of dry sediment} + \text{mass of salt}))/\text{mass of wet sediment} \times 100$$

### 2.2. Grain size analysis

After removing biogenic components (organic matter and $CaCO_3$) from bulk sediments using $H_2O_2$ and HCl, respectively, grain size was analyzed at 4 cm intervals for all sediment cores. Coarser fractions (> 63 μm) were analyzed using a set of sieves and finer fractions (< 63 μm) were analyzed by a Micrometrics Sedigraph 5000 at KOPRI. For samples with small amounts of coarser particles (> 63 μm), the coarser particles (> 63 μm) were treated as 4 phi size. The classification of sediments followed Folk and Ward (1957). The grain size record of core GC02-SS02 was previously reported in Yoon et al. (2005).

To simplify and identify dominant size distributions of all cores, principal component analysis was conducted on frequency percentages from 4 to 11 phi at 1 phi intervals using the Past 3.10 software (Hammer et al., 2001). Grains smaller than 0.5 μm were treated as 11 phi.

### 2.3. Radiocarbon dating

Nine accelerator mass spectrometry (AMS) $^{14}C$ dates were measured from acid insoluble organic matter (AIOM) from core GC03-C2 (Table 2). Five AMS $^{14}C$ dates were measured from AIOM and one AMS $^{14}C$ date from the planktonic foraminifer, *Neogloboquadrina pachyderma* sin., from core GC04-G03 (Table 2). Seven AMS $^{14}C$ dates were measured from AIOM for core GC02-SS02 (Table 2).

## 3. Age model

### 3.1. Core GC02-SS02

An age model for core GC02-SS02 was roughly established by comparing sedimentary facies and geochemical properties with an adjacent core GC02-SS01 (Yoon et al., 2005). Uncorrected $^{14}C$ dates from core GC02-SS02 were not in a chronological order, indicating that these records are not reliable for age model establishment (Table 2). Based on strong correlations between MS values in marine sediments and the EDML ice core $nssCa^{2+}$ record, a high-resolution age model was reconstructed from Scotia Sea sediment cores (e.g., Weber et al., 2012; Xiao et al., 2016). We also correlated the MS values with the EDML ice core $nssCa^{2+}$ record to establish the age model for this core (Fig. 2a). The AnalySeries software (Paillard et al., 1996) was used to produce graphical correlations. Six tie points were constrained for the age model (Table 3, Fig. 2a). A tephra layer at 9–12 cm corresponds to the age (6400–6500 cal. yr BP) of a tephra layer in an adjacent core GC02-SOI03 in the South Orkney Plateau (Tables 1 and 3, Lee et al., 2010).

### 3.2. Core GC03-C2

The uncorrected $^{14}C$ date of the core top is 3563 yr BP, which is older than the reservoir age (1300 year) used in the Scotia Sea (Xiao et al., 2016). Occurrence of old age in the core top is common in the Southern Ocean due to the influence of old carbon (Gordon and Harkness, 1992). Radiocarbon ages of core GC03-C2 continuously

**Table 2**
Accelerator mass spectrometry radiocarbon ages from cores GC02-SS02, GC03-C2, and GC04-G03. The core top age was corrected for corrected age of core GC03-C2 with correction (522 years) of 14 cm core top loss. The calibration program CALIB 7.1 (Stuiver and Reimer, 1993; Reimer et al., 2013) was used to convert the $^{14}C$ ages to calendar ages with a reservoir correction of 1300 years ($\triangle R$ = 900 years) for foraminifers. AIOM: acid insoluble organic matter. *Ages not included in the age model in this study.

| Depth (cm) | Lab code | $^{14}C$ age (yr BP) | Error (yr) | $\delta^{13}C$ (‰) | Corrected and calibrated age (2σ) (cal. yr BP) | Material |
|---|---|---|---|---|---|---|
| GC02-SS02 | | | | | | |
| 0* | NZA18429 | 5673 | ± 44 | −26.0 | | AIOM |
| 110* | NZA18430 | 16,734 | ± 87 | −25.3 | | AIOM |
| 160* | NZA18436 | 12,992 | ± 75 | −25.6 | | AIOM |
| 290* | NZA18518 | 30,261 | ± 307 | −28.0 | | AIOM |
| 340* | NZA18437 | 27,788 | ± 245 | −27.0 | | AIOM |
| 390* | NZA18438 | 34,543 | ± 500 | −24.8 | | AIOM |
| 435* | NZA18439 | 27,936 | ± 257 | −25.9 | | AIOM |
| GC03-C2 | | | | | | |
| 0 | NZA21512 | 3573 | ± 70 | −25.5 | 522 | AIOM |
| 70 | NZA21513 | 6195 | ± 85 | −26.2 | 3132 | AIOM |
| 200 | NZA21514 | 7227 | ± 50 | −26.1 | 4166 | AIOM |
| 320 | NZA21515 | 9394 | ± 40 | −25.5 | 6343 | AIOM |
| 400 | NZA21516 | 9717 | ± 40 | −25.3 | 6669 | AIOM |
| 500 | NZA21578 | 12,296 | ± 50 | −25.6 | 9243 | AIOM |
| 640 | NZA21579 | 16,708 | ± 80 | −25.9 | 13,650 | AIOM |
| 690 | NZA21580 | 19,308 | ± 100 | −26.3 | 16,244 | AIOM |
| 820 | NZA21596 | 21,900 | ± 130 | −26.3 | 18,836 | AIOM |
| GC04-G03 | | | | | | |
| 5* | NZA18439 | 16,304 | ± 65 | −25.0 | | AIOM |
| 38* | NZA18439 | 21,310 | ± 110 | −25.1 | | AIOM |
| 100* | NZA18439 | 25,710 | ± 170 | −25.4 | | AIOM |
| 150* | NZA18439 | 28,030 | ± 220 | −25.2 | | AIOM |
| 200* | NZA18439 | 26,250 | ± 200 | −25.2 | | AIOM |
| 272* | Beta447376 | 26,240 | ± 110 | +0.3 | 29,410 | Planktonic foraminifers |

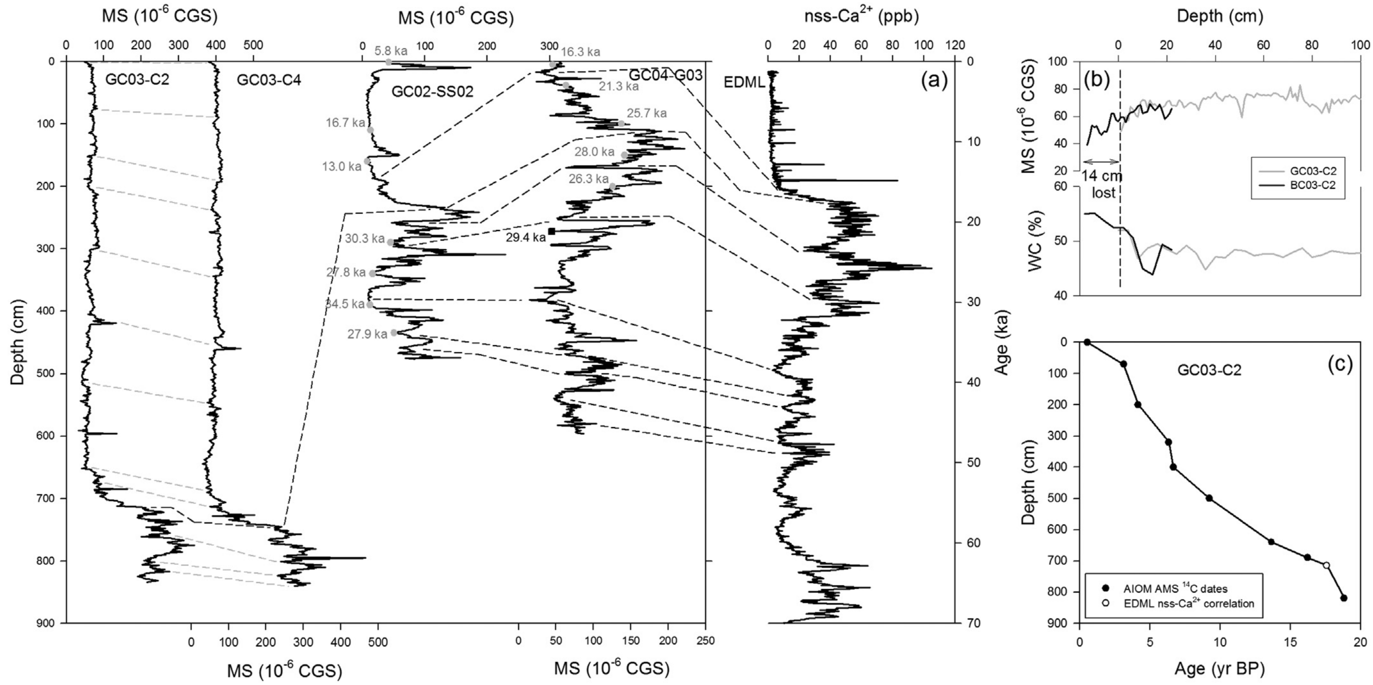

**Fig. 2.** (a) Correlation of magnetic susceptibility (MS) of cores GC02-SS02, GC03-C2, GC03-C4, and GC04-G03 with EDML nssCa$^{2+}$ record (Fischer et al., 2007). Uncorrected $^{14}$C dates of AIOM (gray color) for cores GC02-SS02 and GC04-G03 and calibrated date of planktonic foraminifers (black color) are shown together. (b) Age model for GC03-C2 based on 9 AMS $^{14}$C dates and one MS-EDML nssCa$^{2+}$ tie point. (c) Comparison between box core BC03-C2 and the top 100 cm of core GC03-C2 in order to estimate core top loss of GC03-C2.

**Table 3**
Age tie points of cores GC02-SS02, GC03-C2, GC03-C4, and GC04-G03.

| GC02-SS02 (cm) | GC03-C2 (cm) | GC03-C4 (cm) | GC04-G03 (cm) | Age (yr BP) | Method |
|---|---|---|---|---|---|
| | | 0 | | 522 | MS–GC03-C2 MS |
| | | 98 | | 3244 | MS–GC03-C2 MS |
| | | 192 | | 3768 | MS–GC03-C2 MS |
| | | 237 | | 4166 | MS–GC03-C2 MS |
| | | 342 | | 5962 | MS–GC03-C2 MS |
| 10 | | | | 6500 | Tephra-GC02-SOI03 |
| | | 460 | | 7158 | MS–GC03-C2 MS |
| | | 546 | | 9652 | MS–GC03-C2 MS |
| | | 690 | | 14,273 | MS–GC03-C2 MS |
| | | 713 | | 15,466 | MS–GC03-C2 MS |
| 187 | | | 17 | 15,600 | MS–EDML nssCa$^{2+}$ |
| 234 | 715 | 745 | 112 | 17,600 | MS–EDML nssCa$^{2+}$ |
| | | 772 | | 17,788 | MS–GC03-C2 MS |
| | | 801 | | 18,141 | MS–GC03-C2 MS |
| | | 824 | | 18,588 | MS–GC03-C2 MS |
| | | 836 | | 18,800 | MS–GC03-C2 MS |
| 261 | | | 170 | 23,600 | MS–EDML nssCa$^{2+}$ |
| 296 | | | 253 | 29,500 | MS–EDML nssCa$^{2+}$ |
| 381 | | | 382 | 38,450 | MS–EDML nssCa$^{2+}$ |
| 459 | | | 460 | 41,600 | MS–EDML nssCa$^{2+}$ |
| | | | 500 | 43,000 | MS–EDML nssCa$^{2+}$ |
| | | | 541 | 47,500 | MS–EDML nssCa$^{2+}$ |
| | | | 583 | 48,800 | MS–EDML nssCa$^{2+}$ |

increase with depth (Table 2). This observation may indicate that the variation in old carbon influence was small, which is supported by a narrow range of δ$^{13}$C of dated organic matter, −25.85 ± 0.36‰ (Table 2). This assumption was followed by Lee et al. (2010). As a result, the core top age was subtracted from measured AIOM $^{14}$C dates as a correction for the local reservoir effect and possible old carbon influence (Table 2). Comparing core GC03-C2 with its box core BC03-C2 (Fig. 2b) indicates that approximately 14 cm of GC03-C2 core-top was lost during the coring process. The lost 14 cm of core GC03-C2 was estimated to represent 522 years based on linear extrapolation. Thus, 522 years was considered in the age correction. In addition, we added one tie point (720 cm – 17,600 cal. yr BP) obtained by comparison between the MS values and the EDML ice core nssCa$^{2+}$ record (Fig. 2a). The age model is constructed by nine AMS $^{14}$C dates and one tie point by correlation between the MS values and the EDML ice core nssCa$^{2+}$ record (Fig. 2c).

### 3.3. Core GC03-C4

Although no AMS $^{14}$C dates were measured from this core, the MS variation was very similar to that of core GC03-C2 (Fig. 2a). This finding suggests that the depositional system at these two sites was very similar, due to their proximity. Thus, the age model of core GC03-C4 was established by 13 MS correlation tie points with core GC03-C2 and one MS-EDML dust tie point (Fig. 2a, Table 3).

### 3.4. Core GC04-G03

The uncorrected AIOM $^{14}$C dates of core GC04-G03 were not in a chronological order, indicating that these records were unreliable for constructing an age model (Table 2). We correlated MS values of core GC04-G03 with the EDML ice core nssCa$^{2+}$ record (Fig. 2a). The AnalySeries software (Paillard et al., 1996) was used for graphical correlation. Nine tie points were constrained for the age model for core GC04-G03 (Table 3). The AMS $^{14}$C date of planktonic foraminifers at 272 cm was calibrated using CALIB 7.1 (Stuiver and Reimer, 1993) with the MARINE13 dataset (Reimer et al., 2013). We used 1300 years, previously used in the Scotia Sea (Xiao et al., 2016), as a reservoir correction. The difference at 272 cm between the AMS $^{14}$C date (29,410 cal. yr BP) and the graphical correlation age estimate (30,818 cal. yr BP) is < 1500 years. Considering typical age reconstruction problems in the Southern Ocean, this age difference is thought to be acceptable.

MS profiles of previous sediment cores from the Scotia Sea also typically show a significant amount of core top loss (e.g., Xiao et al.,

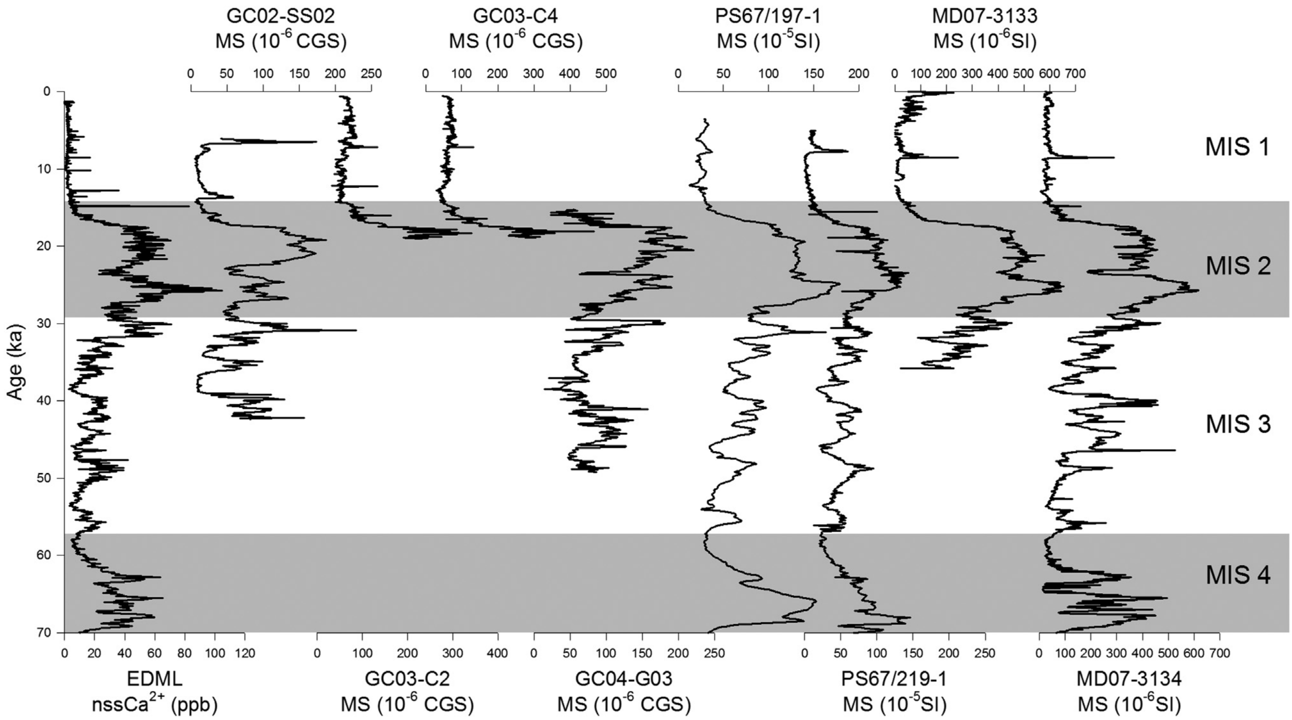


**Fig. 3.** Co-variation between MS values of south Scotia Sea (cores GC02-SS02, GC03-C2, and GC03-C4; this study), northern Powell Basin (core GC04-G03; this study), and central Scotia Sea (cores PS67/197-1, PS67/219-1, MD07-3133, and MD07-3134; Weber et al., 2012; Xiao et al., 2016) with EDML nssCa$^{2+}$ record (Fischer et al., 2007).

2016 and references therein). Very old ages for the uppermost samples are due to core top-loss during the coring process. In addition, the absence of constantly low MS intervals at the top also supports core-top loss.

## 4. Results

MS values of cores GC02-SS02, GC03-C2, GC03-C4, and GC04-G03 were high (up to $> 150 \times 10^{-6}$ CGS) during the last glacial period, especially during Marine Isotope Stage (MIS) 2 (Fig. 3). Although the MS values during MIS 1 were low ($< 100 \times 10^{-6}$ CGS), each core contains at least one MS peak during MIS 1: located at 10 cm and 57 cm at core GC02-SS02, 419 cm at core GC03-C2, and 460 cm at core GC03-C4. The MS variation patterns of all cores are consistent with previous MS records in the Scotia Sea and exhibit a strong correlation with the EDML ice core nssCa$^{2+}$ record (Fig. 3). However, there are differences in peak numbers and amplitudes among all cores, including previously reported cores, in the region (Fig. 3).

Grain size analysis record shows that all cores are composed of silty clay to sandy mud (Figs. 4–7). All cores are characterized by the absence of a gravel-sized fraction, a low proportion of the sand-sized fraction (< 10%), and high proportion of the fine sediment fraction (< 16 μm, 60 to 80%) during MIS 1, except for intermittent MS peak intervals, which are characterized by the opposite during the last glacial period (Figs. 4–7). The mean grain size of all cores was coarser (5 to 6 phi) during the last glacial period than that during MIS 1 (~7 phi). Sand-sized and coarse silt-sized fractions and mean grain size generally co-vary with MS, whereas the fine sediment fraction is anti-correlated with MS in all cores (Figs. 4–7). Gravel-sized fractions appeared in all cores during high MS intervals, but there was no apparent correlation with MS, mean grain size, sand-sized fraction, coarse silt-sized fraction, or clay-sized fraction. The MS values of all size fractions during the glacial period were higher than those during MIS 1 at core GC03-C4 (Fig. 6). However, the MS values were the highest for the coarse silt-sized fraction during the high MS interval (750–840 cm) at core GC03-C4, followed by those of sand-sized and fine sediment fractions (Fig. 6i). In addition, the MS values of the fine to very fine sand (63–250 μm) fraction during the last glacial period (100–200 cm) at core GC04-G03 showed comparable MS values to those of the coarse silt-sized fraction during the last glacial period (750–840 cm) at core GC03-C4 (Figs. 6i and 7i).

Principal component-1 (PC-1), PC-2, and PC-3 account for 74%, 12%, and 7%, respectively, of core GC02-SS02, 67%, 19%, and 11%, of core GC03-C2, 76%, 12%, and 11%, of core GC03-C4, and 93%, 4%, and 2%, of core GC04-G03. Although PC-1 of cores GC02-SS02 and GC04-G03 has a great clay-sized fraction than that of cores GC03-C2 and GC03-C4, PC-1 is generally characterized by finer sediment (mud) and corresponds to the low MS intervals, in particular MIS 1 (Figs. 4–7). In contrast, PC-2 and PC-3, characterized by a higher proportion of 4–6 phi grain sizes with varying amounts of the sand-sized fraction, correspond to the high MS intervals, in particular the last glacial period, except for PC-2 at core GC03-C4 (Figs. 4–7).

## 5. Discussion

### 5.1. Examination of the size fractions responsible for high glacial MS values

The variation patterns of MS for all cores followed variation in the sand-sized fraction and the coarse silt-sized fraction but were anti-correlated to mean grain size (phi) and the fine sediment fraction (Figs. 4–7). This result was statistically confirmed by the correlation coefficient ($r^2$) between the MS values and the mean grain sizes (0.41 for GC02-SS02, 0.69 for GC03-C2, 0.63 for GC03-C4, and 0.42 for GC04-G03), the sand-sized fraction (0.39 for GC02-SS02, 0.87 for GC03-C2, 0.82 for GC03-C4, and 0.55 for GC04-G03), the coarse silt-sized fraction (0.10 for GC02-SS02, 0.21 for GC03-C2, 0.48 for GC03-C4, and 0.14 for GC04-G03), and the fine sediment fraction (0.41 for GC02-SS02, 0.83 for GC03-C2, 0.80 for GC03-C4, and 0.41 for GC04-G03) (Fig. 8). Although the correlation coefficient between the MS values and the coarse silt-sized fraction is not strong, increased

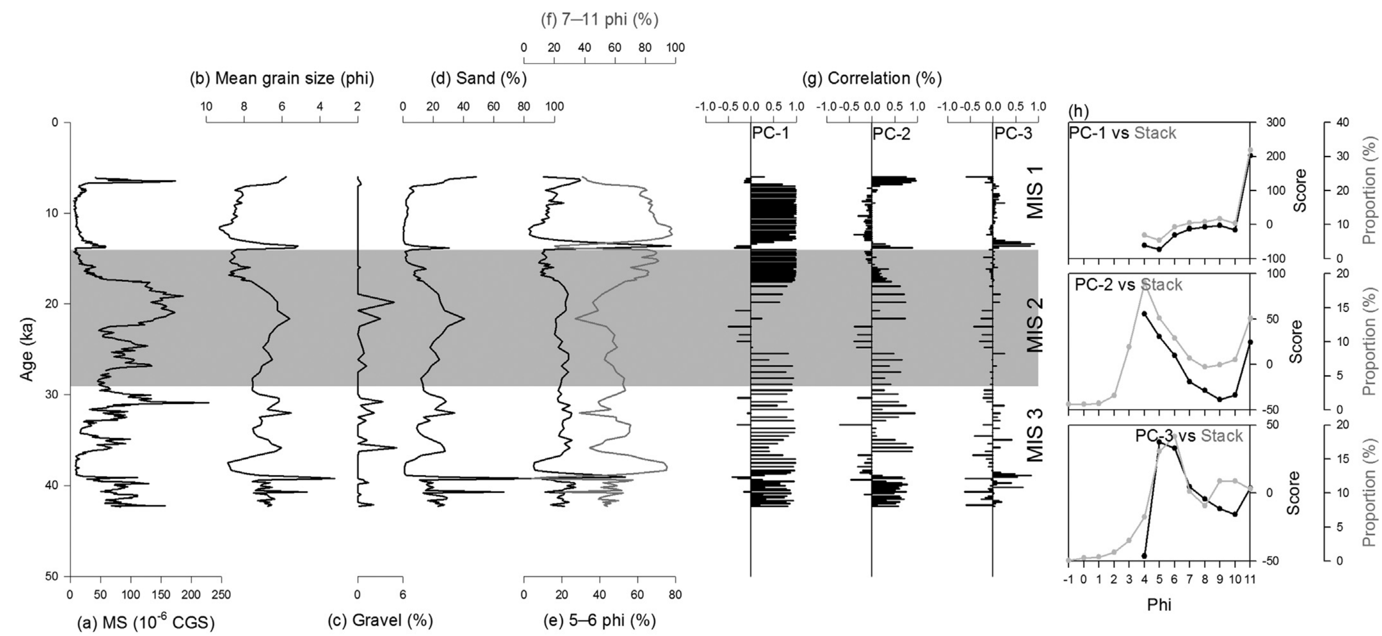


**Fig. 4.** Downcore variations of (a) MS, (b) mean grain size, proportions of (c) gravel, (d) sand, (e) coarse silt (63–16 μm) and fine sediment (< 16 μm), (g) correlation of PCA classes at discrete depths, and (h) grain size distribution of PCA classes and stacked grain size distribution of each PCA class dominant interval at core GC02-SS02.

proportions of the coarse silt-sized fraction together with increases in MS values clearly occur at all cores (Figs. 4–7). High MS value intervals are characterized by increased gravel, sand, and coarse silt and decreased fine sediment (Figs. 4–7). Consequently, our result clearly indicates that the MS values of the Southern Ocean off the northern Antarctic Peninsula are related to a specific grain size fraction ranging from 16 to 250 μm, the fine sand- to coarse silt-sized fraction.

Principal component analysis (PCA) for grain size distribution was applied in order to simplify and identify end members according to different sedimentation processes (e.g., Jonkers et al., 2015). The PCA results for each core reveal that there are three main components for each core, which explain > 95% of the grain size variations. Although there are some differences in distribution patterns of PC-1 among all cores (Figs. 4–7), PC-1 is characterized by higher proportions of fine sediment (< 16 μm) than those of PC-2 and PC-3. PC-1 shows high correlations with grain size distribution during low MS intervals in all cores (Figs. 4–7). In contrast, PC-2 and PC-3 are characterized by higher proportions of sediments > 16 μm (Figs. 4–7). PC-2 and PC-3 show relatively high correlations with grain size distribution during high MS intervals that occur mostly during the glacial period. The MS values at core GC03-C4 during the glacial period were highest in the coarse silt-sized fraction, followed by the sand-sized fraction and fine sediment fraction. In addition, the MS values of the 250–63 μm grains (87% of sand fraction; Fig. 9) at core GC04-G03 revealed comparably high MS

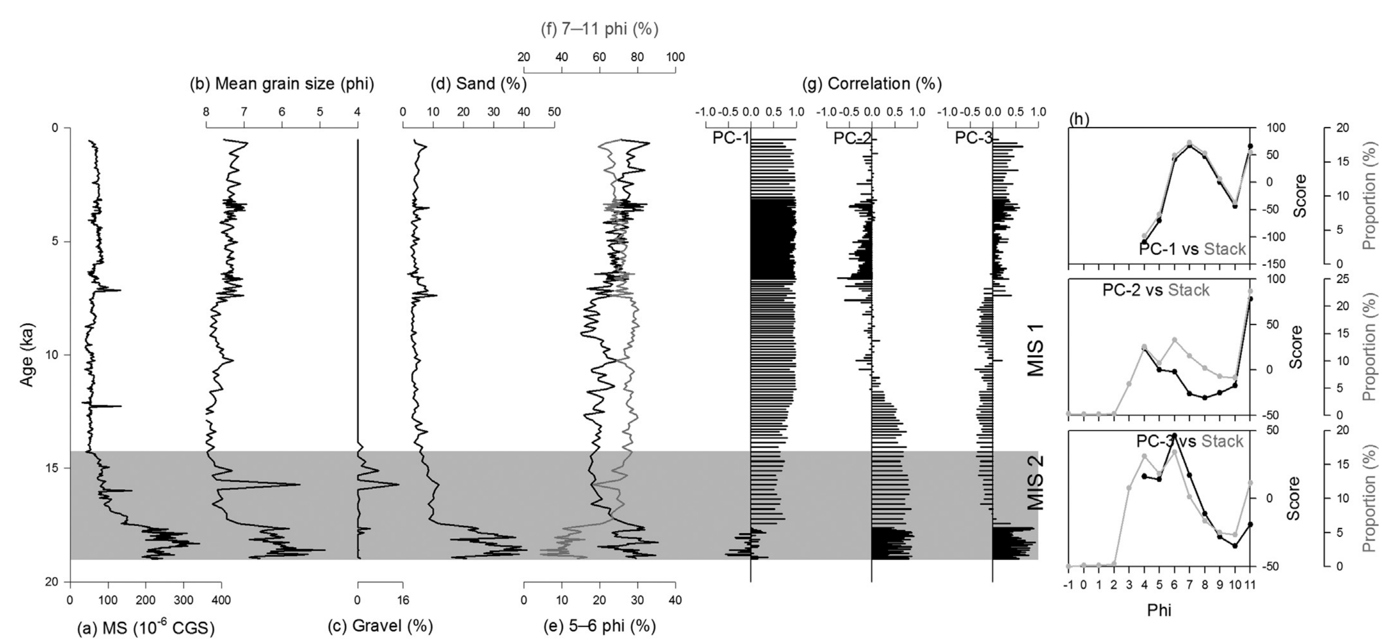


**Fig. 5.** Downcore variations of (a) MS, (b) mean grain size, proportions of (c) gravel, (d) sand, (e) coarse silt (63–16 μm) and fine sediment (< 16 μm), (g) correlation of PCA classes at discrete depths, and (h) grain size distribution of PCA classes and stacked grain size distribution of each PCA class dominant interval at core GC03-C2.

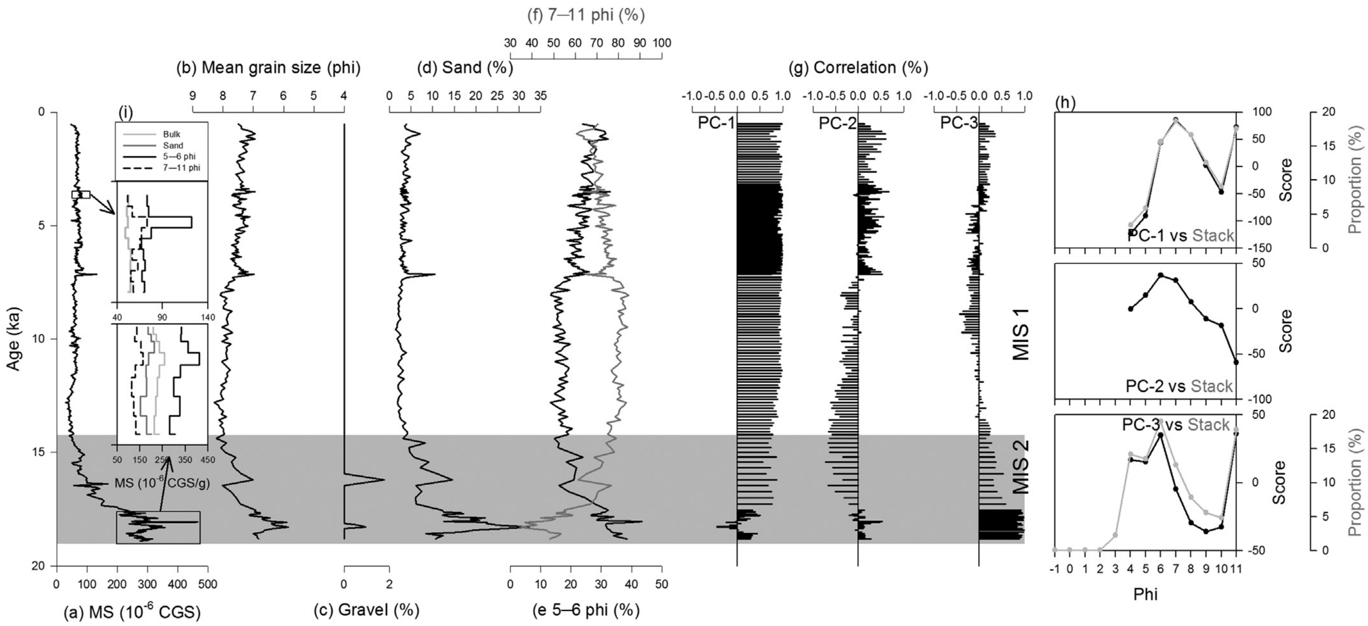


**Fig. 6.** Downcore variations of (a) MS, (b) mean grain size, proportions of (c) gravel, (d) sand, (e) coarse silt (63–16 μm) and fine sediment (< 16 μm), (g) correlation of PCA classes at discrete depths, (h) grain size distribution of PCA classes and stacked grain size distribution of each PCA class dominant interval, and (i) MS values of bulk, sand, coarse silt (63–16 μm), and fine sediment (< 16 μm) at core GC03-C4.

values to those of the coarse silt-sized fraction at core GC03-C4 (Figs. 6i and 7i). This result indicates that increased MS values are ascribed to increased sand- and coarse silt-sized fractions having higher MS values at all cores. Because > 87% of the sand fraction is composed of fine to very fine sand (Fig. 9), sediments ranging from 250 to 16 μm are the main control factor responsible for the increased MS values during the last glacial period.

Although Weber et al. (2012) proposed that MS values of Southern Ocean deep-sea cores are ascribed to dust input from southern South America, the fine sediment fraction of all cores showed a negative correlation with MS (Fig. 4). Although MS values of the fine fraction at core GC03-C4 increased during glacial period compared to MIS 1, the fine sediment fraction has lower MS values than those of the other size fractions (Fig. 6i). This result indicates that the increase in MS values is not related to fine sediment (< 16 μm, i.e., dust). Our records of grain size analysis and MS values indicate that the coarse silt-sized fraction together with the sand-sized fraction most likely control MS variations in marine sediments of the Southern Ocean off the northern Antarctic Peninsula. Although studies on the relationship between the MS values and grain size fractions of previously reported cores do not exist, widespread co-variations of MS in the Southern Ocean off the northern Antarctic Peninsula allow us to anticipate that the MS of these regions is associated with the input of silt- and find sand- sized fractions.

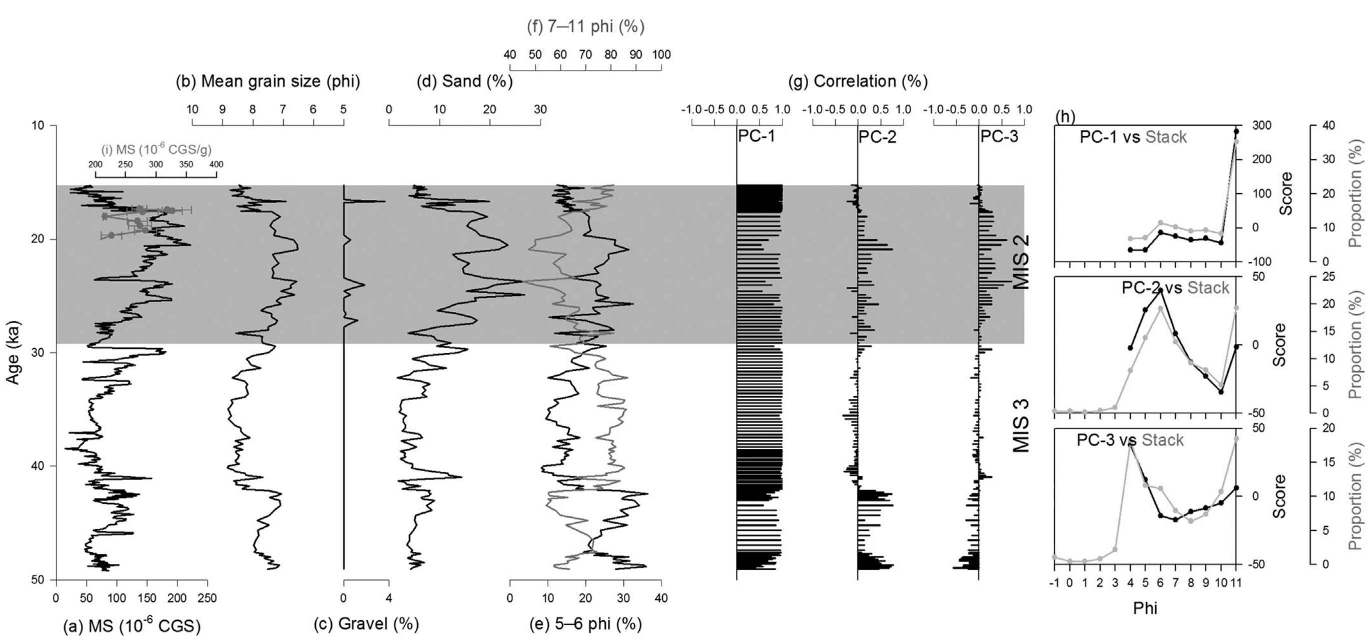


**Fig. 7.** Downcore variations of (a) MS, (b) mean grain size, proportions of (c) gravel, (d) sand, (e) coarse silt (63–16 μm) and fine sediment (< 16 μm), (g) correlation of PCA classes at discrete depths, (h) grain size distribution of PCA classes and stacked grain size distribution of each PCA class dominant interval, and (i) MS values of fine to very fine sand (250–63 μm) at core GC04-G03.

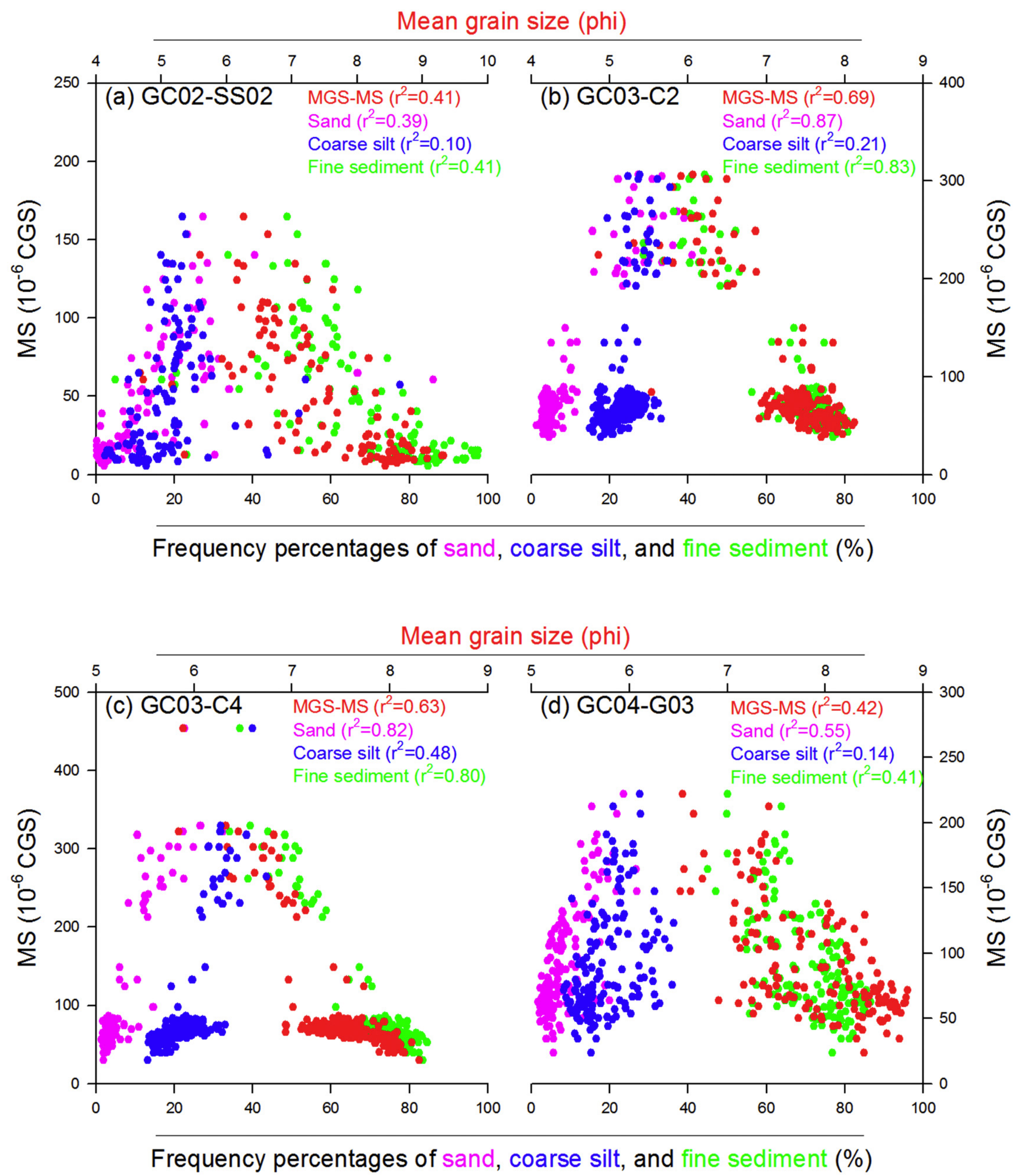


**Fig. 8.** Cross plots between MS and mean grain size and frequency percentages of sand, coarse silt, and fine sediment with $r^2$ values of (a) GC02-SS02 (Yoon et al., 2005), (b) GC03-C2, (c) GC03-C4, and (d) GC04-G03. MGS: mean grain size.

### *5.2. Transport mechanism for the high MS fine sand to coarse silt-sized fraction*

There are strong correlations between the marine sediment MS values in the Scotia Sea and the EDML ice core nss$Ca^{2+}$ record (e.g., Weber et al., 2012; Xiao et al., 2016). In addition, the $Ca^{2+}$ record of sediment core in the Scotia Sea, measured by an AVAATECH X-ray Fluorescence Core Scanner (XRF-CS), was very similar to the EDML nss$Ca^{2+}$ record (Weber et al., 2012). Because the Scotia Sea is located in the trajectory of dust transport from southern South America to East Antarctica, it was proposed that atmospheric circulation (i.e., dust input from the Southern South America) is the major mechanism for controlling MS variation in the Scotia Sea (Weber et al., 2012). However, the similarity between the $Ca^{2+}$ record of sediment cores and the EDML nss$Ca^{2+}$ record does not mean that the terrestrial input ($Ca^{2+}$) is dominated by dust input. Furthermore, Diekmann et al. (2000) reported that fine sediments were not mainly transported from Patagonia by dust input but were transported from various source regions by currents, based on geochemical and mineralogical analysis.

Although it was reported that fine-grained sand is easily transported by wind in the Taklimakan and Gurbantunggut deserts, west China (Sun, 2002), the grain size of the eolian mineral dust that falls in Chinese Loess Plateau and the far-east regions (e.g., the Pacific Ocean, North America, and Greenland) is generally < 75 μm, mostly < 16 μm and < 5% sand-sized grains (Biscaye et al., 1997; Ding et al., 2001). Iriondo (2000) reported that cyclonic winds can transport large amounts of fine-grained sand and silt to the East Patagonian low lands. Although dust fluxes within the southern westerlies were also much higher than those of today during cold periods (Petit et al., 1990), there was no evidence for a significant eolian supply to the Scotia Sea from southern South America (Diekmann et al., 2000). Grains larger than 250 μm are considered within the (sime-)normal distribution pattern of

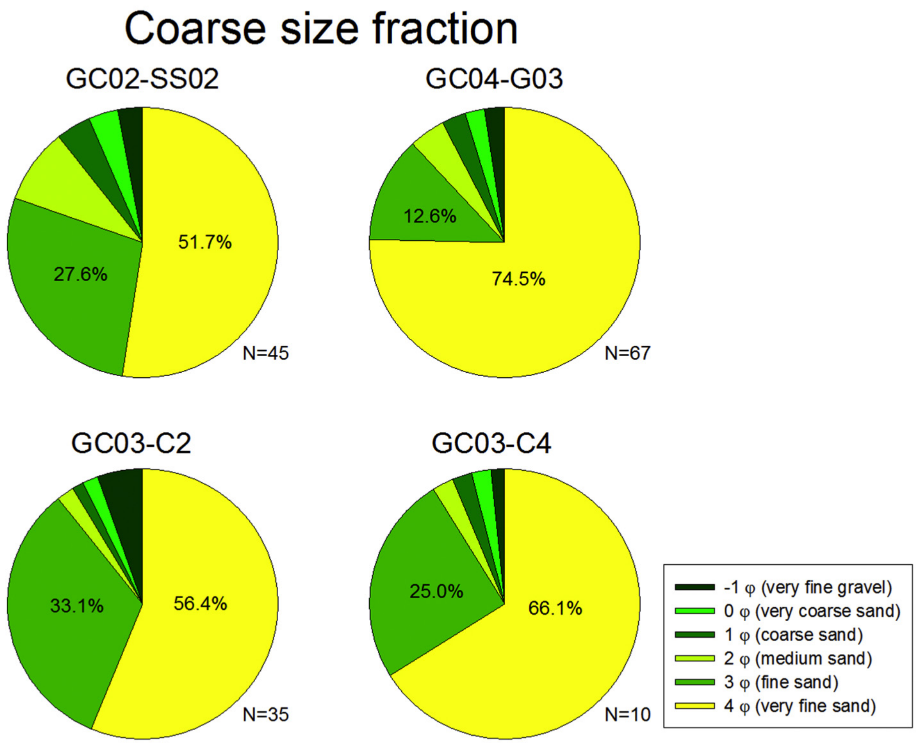


**Fig. 9.** Pie chart of proportions by sand size classification. Number of intervals to calculate proportions by sand size classification is shown together.

PC-2 or PC-3, indicating that these larger grains are transported together with the sand and silt fractions by the same mechanism (Figs. 4h, 5h, 6h, and 7h). Considering that it should be difficult for > 250 μm grains to be transported to the Scotia Sea from south America by wind, the fine sand- to coarse silt-sized fraction with high MS values during the last glacial period is also unlikely to be transported by wind. The fact that there are significant differences in peak numbers and amplitudes of MS values among all cores including previous studies also suggests that eolian supply is not the only explanation (Fig. 3). Dust input is not considered a major controlling factor for MS variations. However, because MS values of fine sediment during the last glacial periods are higher than those during MIS 1, it is plausible that dust input may have contributed to controlling MS variations to some extent.

Hofmann (1999) found a similar MS variation pattern in sediment cores from different current regimes; the MS variation pattern in the south Scotia Sea and the northern Powell Basin (GC04-G03; this study) is also very similar in spite of different regional current systems in these two regions (Orsi et al., 1995). Especially for distal cores in the eastern Scotia Sea, it is unlikely that sand-sized grains are transported by surface currents. Alternatively, the sand-sized fraction can be of volcanic origin probably from the South Sandwich Islands (Nielsen et al., 2007). However, the occurrence of volcanic-related MS peaks was not continuous, but sporadic in Scotia Sea sediments (Xiao et al., 2016). MS peaks at 10 cm of GC02-SS02, at 419 cm of GC03-C2, and at 460 cm of GC03-C4 are volcanic-related during MIS 1 but are not reflected in the EDML dust record (Fig. 10). As a result, concomitant volcanic material input cannot explain the persistently high MS values during the last glacial period.

The widespread appearance of drift deposits and sea floor scouring suggests that bottom and contour currents have an important influence on sedimentation in the Southern Ocean (Diekmann, 2007). The Scotia Sea is influenced by the Weddell Sea Deep Water (WSDW) and the Antarctic Circumpolar Current (ACC), so the bottom water transport must be considered as well. Maldonado et al. (2003) and Gilbert et al. (1998) reported a variety of contourite drifts in the central Scotia Sea and the northwestern Weddell Sea. Yoon et al. (2007) also reported evidence of bottom currents (contourites) from the upper part of core GC02-SS01 and GC02-SS02 in the south Scotia Sea. Because the contourite drifts occurred in areas of weaker flows along the margins of contourite channels (Maldonado et al., 2003), the bottom current most likely acts to entrain and transport fine-grained sediments in the study area. Alternatively, sandy mud layers with high MS values could remain as lag deposits as a result of winnowing of fine sediments by bottom currents. Weak (strong) bottom water strength under a cold (warm) climate was reported in the Antarctic continental margin, including the Weddell Sea and the Ross Sea (Quaia and Brambati, 1997; Gilbert et al., 1998; Brambati et al., 2002). The intervals characterized by high MS values in the Southern Ocean off the northern Antarctic Peninsula were deposited during the last glacial period (Diekmann et al., 2000; Diekmann, 2007; Weber et al., 2012; Xiao et al., 2016; this study). Thus, it is not plausible that wide spread sand-sized fractions during the last glacial period are related to bottom current influence. In addition, different MS values for all grain size fractions between MIS 1 and the last glacial period suggest different sedimentological properties (Fig. 6i).

Because of the proximity of the south Scotia Sea and the Powell Basin to the shelf edge, high MS values during the last glacial period could be related to mass flow deposits, such as turbidites, due to Antarctic ice sheet expansion. However, turbidite deposition was almost absent in all cores during high MS glacial intervals (Fig. 9), which indicates that all core sites are far enough from the shelf to avoid mass flow deposit. The similarity of MS signals between proximal cores of this study and previously reported distal cores (Weber et al., 2012; Xiao et al., 2016) also implies that the mass flow deposit is not the dominant factor for MS variation in the deep Southern Ocean off the northern Antarctic Peninsula (Fig. 3).

There are other transport mechanisms to be considered. Since sea ice acts as a major IRD transport mechanism in the Okhotsk Sea (e.g., Kimura and Wakatsuchi, 1999; Sakamoto et al., 2005, 2006) and our study area is also influenced by sea ice, sea ice must be considered as another potential transport mechanism. However, Weber et al. (2012) argued that sea ice in Antarctica did likely not carry large quantities of

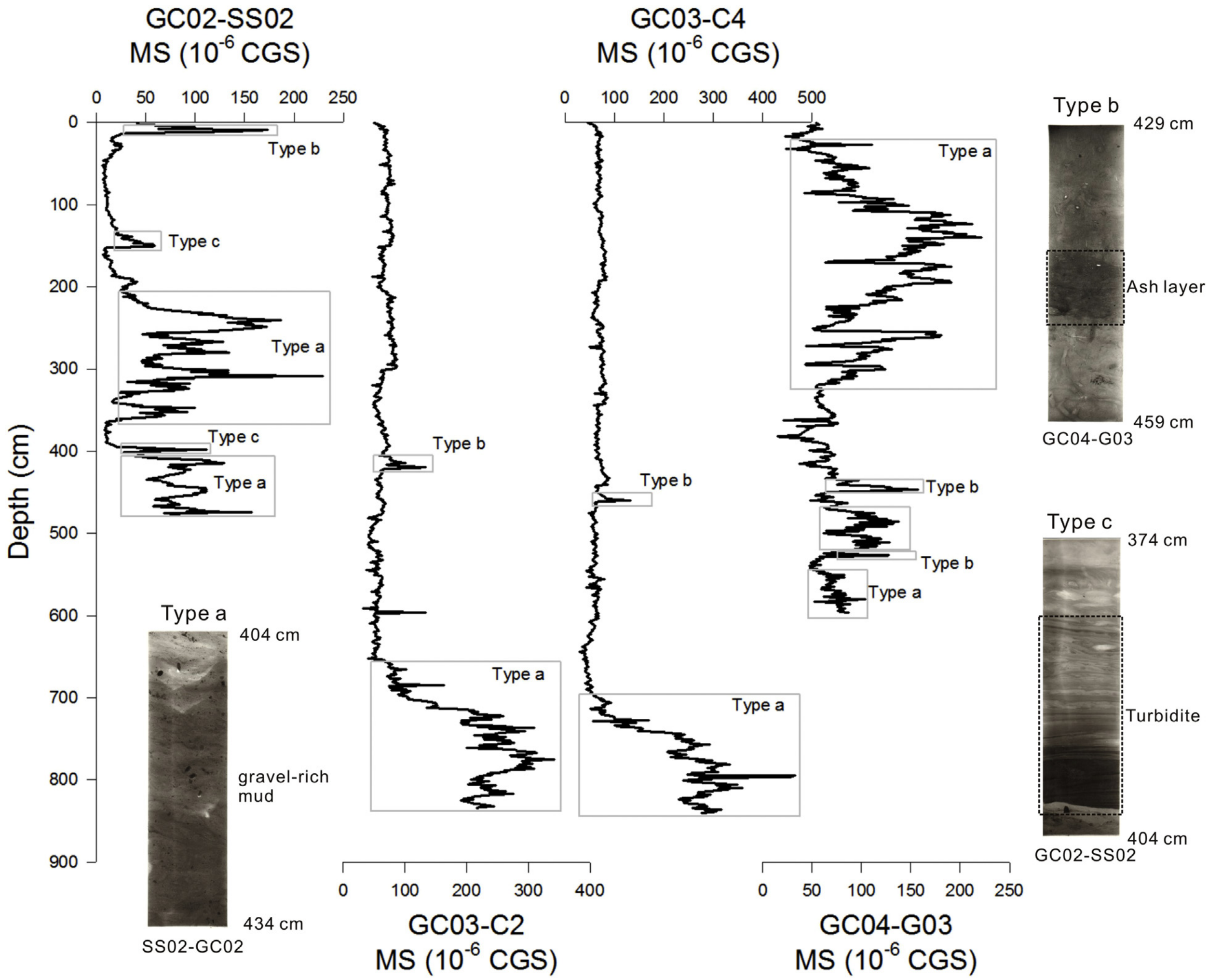


**Fig. 10.** Downcore variation of MS with representative x-ray images of each type for high MS intervals of all cores; type a – gravel-rich mud, type b – ash layer, and type c – turbidite.

fine-grained sediments to the Scotia Sea; the sand-sized fraction is thought to be even more difficult to transport by sea ice. In addition, there was no significant difference in MS values between cores covered by winter sea ice (WSI) and cores not covered by WSI in the Scotia Sea during MIS 1 (e.g., Diekmann et al., 2000; Weber et al., 2012; Xiao et al., 2016), which suggests an insignificant role for sea ice. Nonetheless, because limits of both summer sea ice (SSI) and WSI margins were located farther to the north, especially for WSI (2°N–5°N), during the last glacial period (Allen et al., 2011; Ferry et al., 2015), sea ice may have acted as a supplementary transport mechanism or helped iceberg transport during the last glacial period when MS values are high.

The IRD record, as an indicator for iceberg activity, was compared with the MS values in Scotia Sea sediments (Diekmann et al., 2000; Kanfoush et al., 2000; Weber et al., 2012, 2014). The IRD flux did not match the MS variations, which leads to a conclusion that IRD input has an insignificant role in controlling MS variation in the Scotia Sea. Because IRD is not limited to coarse fraction only (Andrews, 2000; Jonkers et al., 2012, 2015), it should be reconsidered whether grains > 1 mm (Weber et al., 2012) or > 2 mm (Diekmann et al., 2000) in the previous studies are representative of total IRD input. Licht et al. (1999) argued the possibility of a biased gravel-sized fraction in marine sediment because of core diameter limitations. Gravel-sized grains were observed in X-ray photographs of high MS intervals corresponding to the last glacial period in all cores (Fig. 10), indicating an enhanced IRD during the last glacial period. Nonetheless, there were no apparent correlations between the gravel-sized fraction (> 2 mm) and the MS values at all cores (Figs. 4–7). The medium to coarse sand-sized fraction (150 μm to 2 mm) was used for IRD, and prominent IRD intervals were correlated across the Polar Frontal Zone in the southeast Atlantic Ocean during the last glacial period (Kanfoush et al., 2000). In the study of Teitler et al. (2015), the size fraction examined for IRD was also medium to coarse sand (150 μm to 2 mm) in the Southern Ocean. It was reported that > 125 μm detrital components of subpolar sediments in the Northern Hemisphere are considered to originate from icebergs because these larger particles settle rapidly during fluid flow or mass flow (Ruddiman, 1977; Molnia, 1983; Mackiewicz et al., 1984). Grain size distribution of PC-2 and PC-3, dominated by pronounced peaks in coarse silt to fine sand, are very similar to modeled IRD and observed IRD grain size distribution of icebergs in Kongsfjorden (Jonkers et al., 2015). Therefore, sediments ranging mainly from sand to coarse silt with high MS values can be considered as IRD input in the Southern Ocean off the northern Antarctic Peninsula. This assessment is consistent with previous studies; Yoon et al. (2007) proposed that a gravelly sandy mud interval, corresponding to the last glacial period, is likely to result from increased ice rafting in the south Scotia Sea, and Hillenbrand et al. (2009) suggested that the supply of IRD should be reflected by major changes of gravel and sand in marine sediments proximal to the western Antarctic Ice Sheet. Because modeled IRD and observed IRD grain size distribution of icebergs in Kongsfjorden also showed variation in peak grain sizes and the amount of sand-sized grains (Jonkers et al., 2015), we did not sub-divided PC-2 and PC-3 in this study.

The Southern Ocean off the northern Antarctic Peninsula is known as iceberg alley (Anderson and Andrew, 1999). Indeed, the Southern Ocean off the northern Antarctic Peninsula is the most likely location for iceberg detection based on observations from ALTIBERG database (Tournadre et al., 2015) and model results (Merino et al., 2016). In cores GC02-SS02, GC03-C2, GC03-C4, and GC04-G03, located close to the Antarctic Peninsula, IRD is most likely sourced from the Antarctic Peninsula region and Weddell Sea where glaciogenic sediments have high MS values (Diekmann et al., 2000; Yoon et al., 2007). In contrast, IRD at eastern Scotia Sea cores reflects a mixture from southern South America and the Antarctic Peninsula during the last glacial period (Diekmann et al., 2000). Our result is the first record to reveal that variation of MS values is highly dependent on sediment input ranging from coarse silt to fine sand transported as IRD to the Scotia Sea. To confirm our conclusion, comparison between grain size fractions and MS values of previously reported cores from the Scotia Sea is necessary. In addition, different MS values of each size fraction between the low MS interglacial and the high MS glacial period may suggest mineralogical changes (Fig. 6i), which is consistent with the fact that the geochemistry of sediments in the Scotia Sea and the southern Drake Passage is different between glacial and interglacial periods (Diekmann et al., 2000; Walter et al., 2000; Lee et al., 2012). This result suggests that mineralogical studies are also necessary in the future.

### 5.3. Implication of coupling between MS variation and ice core dust record

Graphical correlation between marine sediment MS values and ice core dust records were used to establish high-resolution age construction for sediment cores in the Southern Ocean off the northern Antarctic Peninsula (e.g., Pugh et al., 2009; Allen et al., 2011; Weber et al., 2012; Xiao et al., 2016; this study); this method relies on an assumption that Southern Ocean deep-sea MS values are reliable tracers of atmospheric circulation due to the high MS values of eolian particles from southern South America (Weber et al., 2012). However, which grain size is related to MS variation in marine sediments has not been revealed. Our results show that the input of fine sand- to coarse silt-sized sediments (16–250 μm) with high MS values during glacial period is the main control for the increased glacial MS values in marine cores in the Southern Ocean off the northern Antarctic Peninsula and that the sediments were transported as IRD. Thus, the high MS values during the last glacial period indicate active glacial iceberg calving. The increased iceberg calving activity is attributed to seaward growth of ice masses during glacial periods (Brambati et al., 1991; Strand et al., 1995; DaSilva et al., 1997; Diekmann et al., 2000). This attribution suggests that iceberg calving activity at the margin of the extended ice shelf during the glacial period was high. As a result, a strong correlation between marine sediment core MS values and the ice core dust record indicates that the atmospheric circulation is closely linked to the cryosphere in the Southern Ocean. Because the Southern Ocean off the northern Antarctic Peninsula receives many icebergs (Anderson and Andrew, 1999), a strong correlation between marine sediment MS values with ice core dust records are universally observed in the study area. Nevertheless, graphical correlation can be used for age construction for sediment cores in the Southern Ocean off the northern Antarctic Peninsula.

## 6. Conclusions

The MS values of all cores (GC02-SS02, GC03-C2, GC03-C4, and GC04-G03) from the Southern Ocean off the northern Antarctic Peninsula were high during the last glacial period but were low during MIS 1 and are well correlated to the ice core dust record. Sediments ranging from coarse silt to fine sand (16–250 μm), characterized by high MS values and normal distribution patterns, are considered the main control fraction for MS values in the Southern Ocean off the northern Antarctic Peninsula. These sediments were most likely transported as IRD. Thus, our results suggest that 1) reconsideration about IRD grain size is necessary; 2) iceberg calving activity was active at the margin of extensive glacial ice shelf; and 3) cryosphere (iceberg calving activity) and atmospheric (dust) circulation are closely linked.

## Acknowledgements

We would like to thank the crew and scientific party of the R/V *Yuzhmorgeologiya* for all their help during the gravity coring on board. We would like to thank the KOPRI laboratory members for all their help during experimental measurements. We appreciate the handling editor (Dr. Thierry Correge) and two anonymous reviewers for their critical and constructive comments to improve data interpretation and manuscript structure. This research was supported by KOPRI project (PE18030).

## References

Allen, C.S., Pike, J., Pudsey, C.J., 2011. Last glacial-interglacial sea-ice cover in the SW Atlantic and its potential role in global deglaciation. Quat. Sci. Rev. 30, 2446–2458.
Anderson, J.B., Andrew, J.T., 1999. Radiocarbon constraints on icesheet advance and retreat in the Weddell Sea, Antarctica. Geology 27, 179–182.
Anderson, J.B., Shipp, S.S., Lowe, A.L., Wellner, J.S., Mosola, A.B., 2002. The Antarctic ice sheet during the last glacial maximum and its subsequent retreat history: a review. Quat. Sci. Rev. 21, 49–70.
Andrews, J., 2000. Icebergs and iceberg rafted detritus (IRD) in the North Atlantic: facts and assumptions. Oceangraphy 13 (3), 100–108.
Bailey, I., Hole, G.M., Foster, G.L., Wilson, P.A., Storey, C.D., Trueman, C.N., Raymo, M.E., 2013. An alternative suggestion for the Pliocene onset of major nothern hemisphere glaciation based on the geochemical provenance of North Atlantic Ocean ice-rafted debris. Quat. Sci. Rev. 75, 181–194.
Biscaye, P.E., Grousset, F.E., Revel, M., Van der Gaast, S., Zielinski, G.A., Vaars, A., Kukla, G., 1997. Asian provenance of glacial dust (stage 2) in the Greenland ice sheet project 2 ice Core, summit, Greenland. J. Geophys. Res. 102, 26765–26781.
Brambati, A., Fontolan, G., Simeoni, U., 1991. Recent sediments and sedimentological processes in the Strait of Magelan. Bollettino di Oceanogia Teorica ed Applicata 9, 217–259.
Brambati, A., Melis, R., Quaia, T., Salvi, G., 2002. Late Quaternary climatic changes in the Ross Sea area, Antarctica. Royal Soc. In: Gamble, J.A., Skinner, D.N.B., Henrys, S. (Eds.), Antarctica at the Close of the Millennium. Royala Soc. New Zealand Bull. 35. pp. 359–364 Wellington.
DaSilva, J.L., Anderson, J.B., Stravers, J., 1997. Seismic facies changes along a nearly continuous 24° latitudinal transect: the fjords of Chile and the northern Antarctic peninsula. Mar. Geol. 143, 103–123.
Diekmann, B., 2007. Sedimentary patterns in the Late Quaternary Southern Ocean. Deep-Sea Res. II 54, 2350–2366.
Diekmann, B., Kuhn, G., 1999. Provenance and dispersal of glacial-marine surface sediments in the Weddell Sea and adjoining areas, Antarctica: ice-rafting versus current transport. Mar. Geol. 158, 209–231.
Diekmann, B., Kuhn, G., Rachold, V., Abelmann, A., Brathauer, U., Fütterer, D.K., Gersonde, R., Grobe, H., 2000. Terrigenous sediment supply in the Scotia Sea (Southern Ocean): response to Late Quaternary ice dynamics in Patagonia and on the Antarctic peninsula. Palaeogeogr. Palaeoclimatol. Palaeoecol. 162, 357–387.
Ding, Z.L., Yang, S.L., Hou, S.S., Wang, X., Chen, Z., Liu, T.S., 2001. Magnetostratigraphy and sedimentology of the Jingcuan red clay section and correlation of the Tertiary eolian red clay sediments of the Chinese Loess Plateau. J. Geophys. Res. 106, 6399–6407.
Evans, M.E., Heller, F., 2003. Environmental Magnetism – Principles and Applications of Enviromagnetics, first ed. Academic Press, San Diego.
Ferry, A.J., Crosta, X., Quilty, P.G., Fink, D., Howard, W., Armand, L.K., 2015. First records of winter sea ice concentration in the Southwest Pacific sector of the Southern Ocean. Paleoceanography 30, 1525–1539. http://dx.doi.org/10.1002/2014PA002764.
Fischer, H., Fundel, F., Ruth, U., Twarloh, B., Wegner, A., Udisti, R., Becagli, S., Castellano, E., Morganti, A., Severi, M., Wolff, E., Littot, G., Röthlisberger, R., Mulvaney, R., Hutterli, M.A., Kaufmann, P., Federer, U., Lambert, F., Bigler, M., Hansson, M., Jonsell, U., De Angelis, M., Boutron, C., Siggaard-Andersen, M.-L., Steffensen, J.P., Barbante, C., Gaspari, V., Gabrielli, P., Wagenbach, D., 2007. Reconstruction of millennial changes in dust emission, transport and regional sea ice coverage using the deep EPICA ice cores from the Atlantic and Indian Ocean sector of Antarctica. Earth Planet. Sci. Lett. 260, 340–354.
Folk, R.L., Ward, W.C., 1957. Brazos River bar [Texax]; a study in the significance of grain size parameters. J. Sediment. Res. 27 (1), 3–26.
Gersonde, R., Crosta, X., Abelmann, A., Armand, L., 2005. Sea-surface temperature and sea ice distribution of the Southern Ocean at the EPILOG Last Glacial Maximum – a circum-Antarctic view based on siliceous microfossil records. Quat. Sci. Rev. 24, 869–896.
Gilbert, I.M., Pudsey, C.J., Murray, J.W., 1998. A sediment record of cyclic bottom-current variability from the northwest Weddell Sea. Sediment. Geol. 115, 185–214.
Gordon, J.E., Harkness, D.D., 1992. Magnitude and geographic variation of the

radiocarbon content in Antarctic marine life: implications for reservoir corrections in radiocarbon dating. Quat. Sci. Rev. 11, 697–708.
Haberzettl, T., Anselmetti, F.S., Bowen, S.W., Fey, M., Mayr, C., Zolitschka, B., Ariztegui, D., Mauz, B., Ohlendorf, C., Kastner, S., Lücke, A., Schäbitz, F., Wille, M., 2009. Late Pleistocene dust deposition in the Patagonian steppe – extending and refining the paleoenvironmental and tephrochronological record from Laguna Potrok Aike back to 55 ka. Quat. Sci. Rev. 28, 2927–2939.
Hammer, Ø., Harper, D.A.T., Ryan, P.D., 2001. PAST: paleontological statistics software package for education and data analysis. Palaeontol. Electron. 4, 1–9.
Heroy, D.C., Anderson, J.B., 2005. Ice-sheet extent of the Antarctic peninsula region during the last glacial maximum (LGM)–insights from glacial geomorphology. Geol. Soc. Am. Bull. 117, 1497–1512.
Hillenbrand, C.-D., Baesler, A., Grobe, H., 2005. The sedimentary record of the last glaciation in the western Bellingshausen Sea (West Antarctica): implications for the interpretation of diatictons in a polar-marine setting. Mar. Geol. 216, 191–204.
Hillenbrand, C.-D., Ehrmann, W., Larter, R.D., Benetti, S., Dowdeswell, J.A., Cofaigh, C.Ó., Graham, A.G.C., Grobe, H., 2009. Clay mineral provenance of sediments in the southern Bellingshausen Sea reveals drainage changes of the West Antarctic ice sheet during the Late Quaternary. Mar. Geol. 265, 1–18.
Hofmann, A., 1999. Kurzfristige Llimaschwankungen im Scotiameer und Ergebnisse zur Kalbungsgeschichte der Antarktis während der letzten 200000 Jahre – Rapid Climate oscillations in the Scotia Sea and results of the calving history of Antarctica during the last 200000 years. In: Geowissenschaften. Universität Bremen, Bremen, pp. 178p.
Iriondo, M., 2000. Patagonian dust in Antarctica. Quat. Int. 68, 83–86.
Jonkers, L., Prins, M.A., Moros, M., Weltje, G.J., Troelstra, S.R., Brummer, G.–.J.A., 2012. Temporal offsets between surface temperature, ice-rafting and bottom flow speed proxies in the glacial (MIS 3) northern North Atlantic. Quat. Sci. Rev. 48, 43–53.
Jonkers, L., Barker, S., Hall, I.R., Prins, M.A., 2015. Correcting for the influence of ice-rafted detritus on grain size-based paleocurrent speed estimates. Paleoceanography 30, 1347–1357. http://dx.doi.org/10.1002/2015PA002830.
Kanfoush, S.I., Hodell, D.A., Charles, C.D., Guilderson, T.P., Mortyn, P.G., Ninnemann, U.S., 2000. Millennial-scale instability of the Antarctic ice sheet during the last glaciation. Science 288, 1815–1818.
Kimura, N., Wakatsuchi, M., 1999. Processes controlling the advance and retreat of sea-ice in the sea of Okhotsk. J. Geophys. Res. 104 (C5), 11137–11150.
Lambert, F., Bigler, M., Steffensen, J.P., Hutterli, M., Fischer, H., 2011. The calcium-dust relationship in high-resolution data from Dome C, Antarctica. Clim. Past Discuss. 7, 1113–1137.
Larter, R.D., Anderson, J.B., Graham, A.G.C., Gohl, K., Hillenbrand, C.-D., Jakobsson, M., Johnson, J.S., Kuhn, G., Nitsche, F.O., Smith, J.A., Witus, A.E., Bentley, M.J., Dowdeswell, J.A., Ehrmann, W., Klages, J.P., Lindow, J., Cofaigh, C.O., Spiegel, C., 2014. Reconstruction of changes in the Amundsen Sea and Bellingshausen Sea sector of the West Antarctic ice sheet since the Last Glacial Maximum. Quat. Sci. Rev. 100, 55–86.
Lee, J.I., Bak, Y.S., Yoo, K.C., Lim, H.S., Yoon, H.I., Yoon, S.H., 2010. Climate changes in the South Orkney Plateau during the last 8600 years. The Holocene 20 (30), 395–404.
Lee, J.I., Yoon, H.I., Yoo, K.-C., Lim, H.S., Lee, Y.I., Kim, D., Bak, Y.S., Itaki, T., 2012. Late quaternary glacial-interglacial variations in sediment supply in the southern drake passage. Quat. Res. 78, 119–129. http://dx.doi.org/10.1016/j.yqres.2012.03.010.
Licht, K.J., Dunbar, N.W., Andrews, J.T., Jennings, A.E., 1999. Distinguishing subglacial till and glacial marine diamictons in the western Ross Sea, Antarctica: implications for a last glacial maximum grounding line. Geol. Soc. Am. Bull. 111, 91–103.
Mackiewicz, N.E., Powell, R.D., Carlson, P.R., Molnia, B.F., 1984. Interlaminated ice-proximal glacimarine sediments in Muir inlet, Alaska. Mar. Geol. 57, 113–147.
Maldonado, A., Barnolas, A., Bohoyo, F., Galindo-Zaldívar, Hernández-Molina, J., Lobo, F., Rodríguez-Fernández, Somoza, L., Vázquez, J.T., 2003. Contourite deposits in the central Scotia Sea: the importance of the Antarctic circumpolar current and the Weddell gyre flows. Palaeogeogr. Palaeoclimatol. Palaeoecol. 198, 187–221.
Merino, N., Le Sommer, J., Durand, G., Jourdain, N.C., Madec, G., Mathiot, P., Tournadre, J., 2016. Antarctic icebergs melt over the Southern Ocean: climatology and impact on sea ice. Ocean Model 104, 99–110. http://dx.doi.org/10.1016/j.ocemod.2016.05.001.
Minzoni, R.T., Anderson, J.B., Fermandez, R., Wellner, J.S., 2015. Marine record of Holocene climate, ocean, and cryosphere interactions: Herbert sound, James Ross Island, Antarctica. Quat. Sci. Rev. 129, 239–259.
Molnia, B.F., 1983. Distal glacial marine sedimentation: abundance, composition and distribution of North Atlantic Pleistocene ice rafted sediment. In: Molnia, B.F. (Ed.), Glacial Marine Sedimentation. Plenum Press, New York, pp. 593–626.
Nakada, M., Kimura, R., Okuno, J., Moriwaki, K., Miura, H., Maemoku, H., 2000. Late Pleistocene and Holocene melting history of the Antarctic ice sheet derived from sea-level variations. Mar. Geol. 167, 85–103.
Nielsen, S.H.H., Hodell, D.A., Kamenov, G., Guilderson, T., Perfit, M.R., 2007. Origin and significance of ice-rafted detritus in the Atlantic sector of the Southern Ocean. Geochem. Geophys. Geosyst. 8, 1–23.
Orsi, A.H., Whitworth, T., Nowlini Jr., W.D., 1995. On the meridional extent and fronts of the Antarctic circumpolar current. Deep Sea Res., Part I 42 (5), 641–673.
Paillard, D., Laeyrie, L., Yiou, P., 1996. Macintosh program performs time-series analysis. In: EOS Transactions American Geiophysical Union, Washington D.C. Vol. 77. pp. 379.
Peck, V.L., Hall, I.R., Zahn, R., Grousset, F., Hemming, S.R., Scourse, J.D., 2007. The relationship of Heinrich events and their European precursors over the past 60 ka BP: multi-proxy ice-rafted debris provenance study in the north East Atlantic. Quat. Sci. Rev. 26, 862–875. http://dx.doi.org/10.1016/j.quascirev.2006.12.002.
Peck, V.L., Allen, C.S., Kender, S., McClymont, E.L., Hodgson, D.A., 2015. Oceanographic variability on the West Antarctic peninsula during the Holocene and the influence of upper circumpolar deep water. Quat. Sci. Rev. 119, 54–65.
Petit, J.R., Mounier, L., Jouzel, J., Korotkevitch, Y., Kotlyakov, V., Lorius, C., 1990. Paleoclimatological implications of the Vostok core dust record. Nature 343, 56–58.
Pugh, R.S., MaCave, I.N., Hillenbrand, C.–.D., Kuhn, G., 2009. Circum-Antarctic age modeling of quaternary marine cores under the Antarctic circumpolar current: ice-core dust-magnetic correlation. Earth Planet. Sci. Lett. 284, 113–123.
Quaia, T., Brambati, A., 1997. Climatic stages control on grain-size clusters in core ANTA91–8 (Ross Sea). Geografia Fisica Geodinam Quatern 20, 279–282.
Reid, D.E., Anderson, J.B., 1990. Hazards to Antarctic exploration and production, in Antarctic as an Exploration Frontier. In: St. John, B. (Ed.), Hydrocarbon Potential Geology and Hazards. 31. American Association of Petroleum Geologists Studies in Geology, Tulsa, Oklahoma, pp. 31–46.
Reimer, P.J., Bard, E., Bayliss, A., Beck, J.W., Blackwell, P.G., Ramsey, C.B., Buck, C.E., Cheng, H., Edwards, R.L., Friedrich, M., Grootes, P.M., Guilderson, T.P., Haflidason, H., Hajdas, I., Hatté, C., Heaton, T.J., Hoffmann, D.L., Hogg, A.G., Hughen, K.A., Kaiser, K.F., Kromer, B., Manning, S.W., Niu, M., Reimer, R.W., Richards, D.A., Scott, E.M., Southon, J.R., Staff, R.A., Turney, C.S.M., van der Plicht, J., 2013. IntCal13 and Marine13 Radiocarbon age calibration curves 0–50,000 years cal BP. Radiocarbon 55, 1869–1887.
Röthlisberger, R., Bigler, M., Wolff, E.W., Joos, F., Monnin, E., Hutterli, M.A., 2004. Ice core evidence for the extent of past atmospheric $CO_2$ change due to iron fertilisation. Geophys. Res. Lett. 31, L16207. http://dx.doi.org/10.1029/2004GL020338.
Ruddiman, W.F., 1977. Late quaternary deposition of ice-rafted sand in the subpolar North Atlantic (late 40 to 65 N). Geol. Soc. Am. Bull. 88, 1813–1827.
Sakamoto, T., Ikehara, M., Aoki, K., Iijima, K., Kimura, N., Nakatsuka, T., Wakatsuchi, M., 2005. Ice-rafted debris (IRD)-based sea-ice expansion events during the past 100 kyrs in the Okhotsk Sea. Deep-Sea Res. II 52, 2275–2301.
Sakamoto, T., Ikehara, M., Uchida, M., Aoki, K., Shibata, Y., Kanamatsu, T., Harada, N., Iijima, K., Katsuki, K., Asahi, H., Takahashi, K., Sakai, H., Kawahata, H., 2006. Millennial-scale variations of sea-ice expansion in the southwestern part of the Okhotsk Sea during the past 120 kyr: age model and ice-rafted debris in IMAGES Core MD01-2412. Glob. Planet. Chang. 53, 58–77.
Strand, K., Marsaglia, K., Forsythe, R., Kurnosov, V., Vergara, H., Lewis, S.D., Behrmann, J.H., Musgrave, R.J., Gande, S.C., 1995. Outer margin depositional systems near the Chile margin tripple junction. In: Proceedings ODP, Scientific Results. Ocean Drilling Program, College Station, TX, pp. 379–397.
Stuiver, M., Reimer, P.J., 1993. Extended 14C database and revised CALIB radiocarbon calibration program. Radiocarbon 35, 215–230.
Sun, J.M., 2002. Source regions and formation of the loess sediments on the high mountain regions of northwestern China. Quat. Res. 58, 341–351.
Takahashi, T., Sutherland, S.C., Sweeney, C., Poisson, A., Metzl, N., Tilbrook, B., Bates, N., Wanninkhof, R., Feely, R.A., Sabine, C., Olafsson, J., Nojiri, Y., 2002. Global sea-air $CO_2$ flux based on climatological surface ocean $pCO_2$, and seasonal biological and temperature effects. Deep-Sea Res. II 49, 1601–1622.
Teitler, L., Florindo, F., Warnke, D.A., Filippelli, G.M., Kupp, G., Taylor, B., 2015. Antarctic ice sheet response to a long warm interval across marine isotope stage 31: a cross-latitudinal study of iceberg-rafted debris. Earth Planet. Sci. Lett. 409, 109–119.
The RAISED Consortium et al., 2014. A community-based geological reconstruction of Antarctic ice sheet deglaciation since the last glacial maximum. Quat. Sci. Rev. 100, 1–9.
Tournadre, J., Bouhier, N., Girard-Ardhuin, F., Rmy, F., 2015. Large icebergs characteristics from altimeter waveforms analysis. J. Geophys. Res. 120, 1954–1974. http://dx.doi.org/10.1002/2014JC010502.
Walter, H.J., Hegner, E., Diekmann, B., Kuhn, G., Rutgers van der loeff, M.M., 2000. Provenance and transport of terrigenous sediment in the South Atlantic Ocean and their relations to glacial and interglacial cycles: Nd and Sr isotopic evidence. Geochim. Cosmochim. Ac. 64, 3813–3827.
Weber, M.E., Kuhn, G., Sprenk, D., Rolf, C., Ohlwein, C., Ricken, W., 2012. Dust transport from Patagonia to Antarctica – a new stratigraphic approach from the Scotia Sea and its implications for the last glacial cycle. Quat. Sci. Rev. 36, 177–188.
Weber, M.E., Clark, P.U., Kuhn, G., Timmermann, A., Sprenk, D., Gladstone, R., Zhang, X., Lohmann, G., Menviel, L., Chikamoto, M.O., Friedrich, T., Ohlwein, C., 2014. Millennial-scale variability in Antarctic ice-sheet discharge during the last deglaciation. Nature 510, 134–138.
Xiao, W., Frederichs, T., Gersonde, R., Kuhn, G., Esper, O., Zhang, X., 2016. Constraining the dating of late quaternary marine sediment records from the Scotia Sea (Southern Ocean). Quat. Geochronol. 31, 97–118. http://dx.doi.org/10.1016/j.quageo.2015.11.003.
Yoon, H.I., Nam, S.H., Yoo, K.-C., Park, B.-K., Kim, Y., Oh, J.-K., 2005. Late quaternary paleoceanographic change in the south Scotia Sea, northern Antarctic peninsula. J. Geol. Soc. Korea 41, 211–226 (in Korean with English abstract).
Yoon, H.I., Khim, B.K., Yoo, K.-C., Bak, Y.S., Lee, J.I., 2007. Late glacial to Holocene climatic and oceanographic record of sediment facies from the south Scotia Sea off the northern Antarctic peninsula. Deep-Sea Res. II 54, 2367–2387.